Experimentally identifying masked sources applying time reversal with the selective source reduction method

B. E. Anderson,[1,a] T. J. Ulrich,[1] M. Griffa,[1,b] P.-Y. Le Bas,[1] M. Scalerandi,[2] A. S. Gliozzi,[2] and P. A. Johnson[1]

[1]*Geophysics Group, Los Alamos National Laboratory, Los Alamos, New Mexico 87544, USA*
[2]*Department of Physics, CNISM, Politecnico di Torino, C.so Duca degli Abruzzi 24, 10129 Torino, Italy*

This paper describes a time reversal (TR) method of spatially illuminating a source signal which has been masked by another source signal. This masking occurs as a result of inherent limitations in the traditional TR process. The selective source reduction (SSR) method employs a subtraction technique where one TR focus is selectively reduced to illuminate the masked focus. Experimental results and considerations are presented to demonstrate the SSR method for two elastic wave pulses emitted simultaneously from two spatially separated surficial sources and to examine the limitations of the method. A blind test was conducted to demonstrate that no *a priori* information about the source(s) is required. Spatial and/or temporal characteristics of multiple close-proximity sources can be resolved with the use of the illumination method. The measurements show that the SSR method's limitations are chiefly due to imperfect temporal reconstruction of the source function in the time reversed focal signal, which consequently limits signal reduction. © *2009 American Institute of Physics*. [DOI: 10.1063/1.3079517]

I. INTRODUCTION

In blind, multiple, or complex source problems, such as in earthquakes and crack detection for nondestructive evaluation (NDE), time reversal (TR) may be used to reconstruct the complex source(s).[1,2] In fact, TR is a method of focusing energy onto a specific location in space and time,[3–5] hence providing the tools for spatial localization and temporal reconstruction of the original source(s). The main application areas of TR include nondestructive testing, earthquake characterization, underwater acoustics, biomedical ultrasound, and audio acoustics. A restriction in the application of TR is given by the limit in spatial focusing due to diffraction processes which greatly affects the reconstruction ability of TR for complex sources whose individual components are in close proximity in space and time. Some currently available methods allow one to improve upon the limitations inherent in complex source reconstruction using TR, through the achievement of super-resolution, but they require modification of the source or medium (e.g., addition of nearfield scatterers[6]) and/or *a priori* knowledge of the source signal(s) (e.g., using an acoustic sink[7,8]).

The selective source reduction (SSR) method selectively eliminates or reduces in amplitude a time reversed focal signal that is masking another time reversed focal signal.[9] This method can be successfully accomplished with a single receiving transducer, although additional receivers should improve the results. In the standard implementation of TR, a source or sources emit forward signals, which propagate through the medium and are detected, time reversed, and sent back to the source(s) from a set of receivers/transducers placed in the specimen, referred to as the TR mirror (TRM). For a complex source, it is conceivable that a reconstructed strong source may mask a nearby reconstructed weak source (or two close-proximity and equal amplitude sources may mask each other by merging into a single focus).

In addition, the use of a finite number of TRM elements, especially if arranged in an (one dimensional or two dimensional) array configuration, imposes a limited spatial sampling of the forward propagation wave fields. The spatial sampling introduces some artifacts in the final snapshots of the TR focused wave fields, known as side lobes (including aliased grating lobes) in the field of array processing[10] and of relevant importance, among others, in interferometric radio astronomy,[11] ocean acoustics,[12] and radar.[13] A side lobe may have higher amplitude than a focal spot associated with a real source, thereby masking it.

Throughout this paper we will consider only two sources for simplicity, but the extension to multiple sources should follow in a straightforward manner provided that the noise floor is not an issue. The SSR method does not attempt to handle the problem of removing spurious side lobes. Other techniques have been developed for that purpose in the field of array processing. For example, in ocean acoustics, different beamforming techniques, under the common name of matched field (MF) processing,[12,14–16] have been developed for localizing sources in space with simultaneous minimization of the side lobe artifacts. In interferometric radio astronomy, an algorithm called CLEAN has been devised for the same purpose.[11,17] CLEAN has also been combined with a MF processor for an optimal source imaging.[18] Parts of these techniques can be combined with SSR for high resolution imaging of sources. This combination is, however, beyond the scope of this work.

The method proposed here is based on the consideration

---

[a]Electronic mail: bea@byu.edu.
[b]Electronic mail: michele.griffa@empa.ch, EMPA, Swiss Fed. Lab. for Mat. Test. and Res., Bldg. Tech. Lab., Dübendorf, 8600, Switzerland.

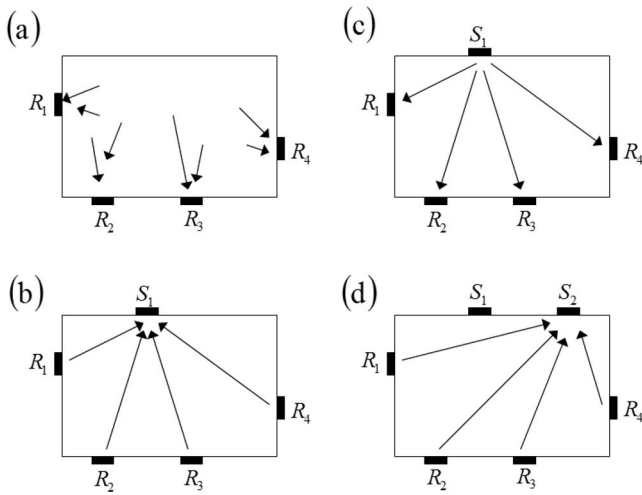FIG. 1. Schematic of the SSR method using TR. Sources and receivers are denoted by S ($S_1 > S_2$) and R, respectively. Subplots (a) and (b), respectively, display the forward propagation and back propagation from a typical TR experiment. The additional forward propagation and back propagation steps required by SSR are depicted in subplots (c) and (d), respectively.

that the forward detected signal(s) from two unknown sources should contain information from each source. Our aim is to determine, with an experimental procedure and without *a priori* knowledge about the medium, one of the two contributions and suppress it in favor of the other. For this purpose, in the SSR method, the strongest time reversed focused signal is detected after a standard implementation of TR [forward propagation depicted in Fig. 1(a) and back propagation depicted in Fig. 1(b)]. The strongest focal signal is time reversed and windowed (everything but the focus is windowed out), ideally constituting a reconstruction of the time dependence of the dominant source. The reversed and windowed signal is then broadcast into the medium from the position of the strongest source and the response is detected by the same set of receivers used in the original implementation of TR [depicted in Fig. 1(c)]. The resulting signal(s) should then contain information from only the strongest source. The two sets of detected forward propagation signals are then vector normalized and subtracted leaving, ideally, only the direct arrival and coda (i.e., the portion of the signal composed of multiple reflections) from the weaker source. In the final step, the subtracted signal(s) are time reversed and broadcast into the medium by the TRM ideally focusing only at the position of the weaker source. The focus at the stronger source has been eliminated or reduced [depicted in Fig. 1(d)]. In this manner the weaker source can be characterized.

The theory of SSR has been presented by Scalerandi *et al.*,[9] including numerical simulations and a preliminary controlled experimental verification to illustrate the procedure. However, in that work, knowledge of the two source locations was available *a priori*. On the contrary, the experimental contributions of the current work include a true blind test to identify source locations (where the locations and times of emission were unknown *a priori*), an investigation of the limitations of sources in close spatial proximity, and an investigation of the limitations due to system noise and relative strengths of sources. The sources considered in this experi-

mental work are strictly surficial sources; however, the SSR method is not theoretically limited to surficial sources, if combined with simulations of the backward propagation. Additional insights into practical implementation of the SSR method are given in this paper. In particular, the reason for the remnant at the focal time at the dominant source after performing SSR (which occurs in both modeling and experimental results) is fully explained, whereas in the work of Scalerandi *et al.* this phenomena was not investigated [see Figs. 6(a), 7(a), 9(a), 10(a), and 14(c) of Ref. 9].

II. EXPERIMENT SETUP

Two samples were used in different experiments presented and discussed in Secs. II and IV (a third sample was used in Sec. V and described in that section): a silica glass cube measuring 10 cm in each direction and a doped glass block measuring $10.16 \times 8.89 \times 8.78$ cm^3. Both samples had piezoelectric ceramic transducers bonded to them with 5 Minute® epoxy. The transducers used on the silica glass cube were 1 MHz resonance PZT-5H ceramic transducer disks, measuring 2 mm in thickness and a diameter of 12.7 mm. The transducer used on the doped glass block was a 3 mm diameter and 2 mm thick PZT-5 ceramic transducer disk. Photographs of these samples may be found in Fig. 2, with the silica glass block depicted in Fig. 2(a), and the doped glass block depicted in Fig. 2(b). The transverse wave speed, which dominates the wave energy in the out of plane direction, in the silica glass cube is approximately 3782 m/s, while the transverse wave speed in the doped glass block is approximately 2347 m/s. The center frequencies used in each sample were 250 and 200 kHz, respectively (corresponding to 15.1 and 11.7 mm wavelengths).

In each experimental demonstration of the SSR method presented in this paper, electronic sine wave signals, modulated by a sine squared envelope, were used as source signals,

$$u(t) = A \sin^2\left(\frac{\pi}{\Delta\tau}t\right)\sin(2\pi ft), \tag{1}$$

where A is the amplitude, $\Delta\tau$ is the pulse width, t is time, and f is the sine wave frequency. It should be stressed here that successful implementation of the SSR method does not require source signals defined in this way.

The experiments described in this paper employed the use of "virtual" sources. A virtual source is created by sending energy from a transducer located at the position A into the sample. A laser vibrometer detects the vibration velocity at a certain point B (that may be user defined). The principle of reciprocity states that one obtains the same result by sending a signal from point A and recording it at B or sending the same signal from B to point A.[19–22] Therefore, the experiment is the equivalent of having a virtual source at B and receiving the signal at A. The advantage is that the transducer used in a virtual source experiment may be considered to be the TRM. The velocity signal detected by the laser is time reversed and injected into the sample by the transducer. Thus a time reversed focus is created at the laser's position. A virtual source has thus been reconstructed at the laser's
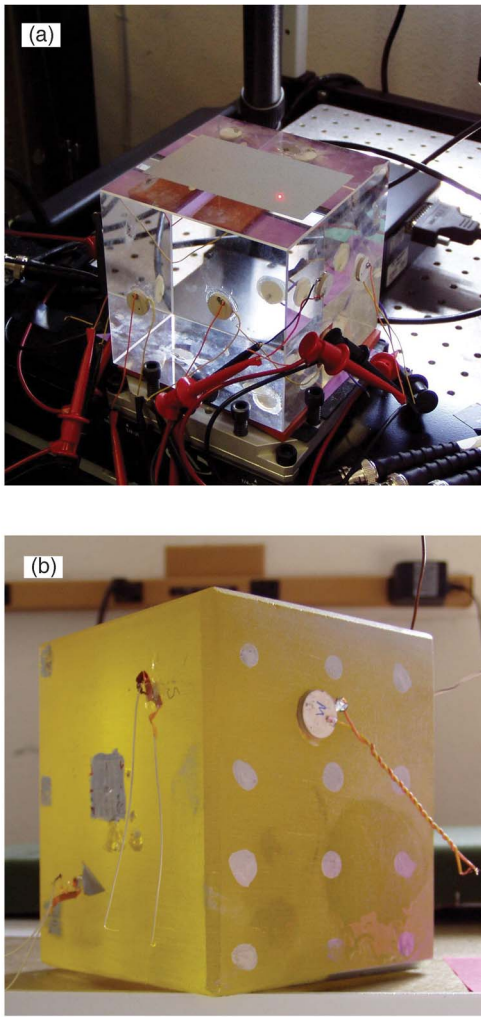
FIG. 2. (Color online) Photographs of the two samples used in the experiments described in this paper. Subplot (a) displays the silica glass cube sample and subplot (b) displays the doped glass block sample.

position. The virtual source method not only provides a simplification of a standard TR experiment (skipping the swapping operation of the transducers) but it also allows the user to focus energy at a selected point on the sample.

The same procedure can be implemented using multiple transducers: the emission from each TRM transducer is done separately, each of them injecting the same signal. Then the set of signals measured by the laser vibrometer constitutes the set of signals that would have been measured by each TRM transducer had the source emission been emitted from the position of the laser vibrometer. They are time reversed and broadcast simultaneously each from the corresponding transducers, thus obtaining an improved focusing on the laser position. In our experiments we have generated virtual sources using a single transducer for the doped glass block and eight transducers in the case of the silica glass block. The TRM transducers are placed randomly on the sample's surface to avoid the aliasing effects due to regular transducer array spacing.

The details of the implementation of SSR experiments employing the virtual source method in the laboratory will now be described. To generate two surficial, virtual sources

in separate positions, we have adopted the following procedure. The pulse signal described by $u(t)$ [a typical signal is displayed in Fig. 3(a)] was transmitted from each TRM transducer separately to obtain the set of signals, $v_i^{(1)}(t)$ [a typical signal is displayed in Fig. 3(b)], recorded in a position S_1. The signals recorded at the TRM correspond to a virtual source emission from a position S_1. Then the procedure is identically repeated, recording in a different position S_2 the signals $v_i^{(2)}(t)$ [a typical signal is displayed in Fig. 3(c)] corresponding to a virtual source emission from a second position S_2. The sets of signals $v_i^{(1)}(t)$ and $v_i^{(2)}(t)$ are linearly combined with different relative contributions to simulate the signals recorded by a set of TRM transducers, $v_i^{(1+2)}(t)$, due to the emissions of two potentially differing amplitude sources,

$$v_i^{(1+2)}(t) = A_1 v_i^{(1)}(t) + A_2 v_i^{(2)}(t), \qquad (2)$$

with $A_1 \geq A_2$. The signals $v_i^{(1+2)}(t)$ are then time reversed [a typical signal is displayed in Fig. 3(d)] and broadcast from the TRM transducers.

Since in our problem the existence of the source(s) and the position(s) of the source(s) is unknown, a preliminary detection step is required. The surface of the medium/sample must be sampled by one or more receivers monitoring the temporal wavefield (i.e., in the case of NDE a surface of the sample may be scanned with a laser vibrometer). In the case of buried sources, the rest of the procedure must be carried out numerically with a model of the medium/sample. Once a source or sources are detected, it is then known that the classical TR experiment described in the previous paragraph yields focusing, at least on the strongest source, thus allowing one to locate S_1. The focal signal $w_1(t)$ at the S_1 location is then extracted [a typical signal is displayed in Fig. 3(e)]. In the case of a strong source whose TR reconstruction masks the TR reconstruction of a smaller source, no evidence of focusing at S_2 is apparent and the reconstruction $w_2(t)$ is not possible. Then, as Scalerandi *et al.*[9] proposed in Sec. VA of their paper, the selected focal signal is time reversed and windowed such that only the focal waveform remains, $w_1'(t)$. A typical signal is displayed in Fig. 3(f), which is ideally a reconstruction of the original source signal [compare Fig. 3(f) with Fig. 3(a)]. Thus the first TR process has been completed.

During the second TR process, the signal $w_1'(t)$ is used in a virtual source experiment. Each TRM transducer broadcasts $w_1'(t)$ separately and the response is measured by the laser vibrometer at the position of S_1. We call this set of signals $x_i^{(1)}(t)$ [a time reversed typical signal is displayed in Fig. 3(g)]. The two sets of received signals, $v_i^{(1)}(t)$ and $x_i^{(1)}(t)$, are then vector normalized (meaning the signal is divided by the square root of the sum of the squares of each value in the signal) and subtracted from one another to produce $y_i(t)$, where

$$y_i(t) = \frac{v_i^{(1+2)}(t)}{\sqrt{\sum_k [v_i^{(1+2)}(t_k)]^2}} - \frac{x_i^{(1)}(t)}{\sqrt{\sum_k [x_i^{(1)}(t_k)]^2}}. \qquad (3)$$
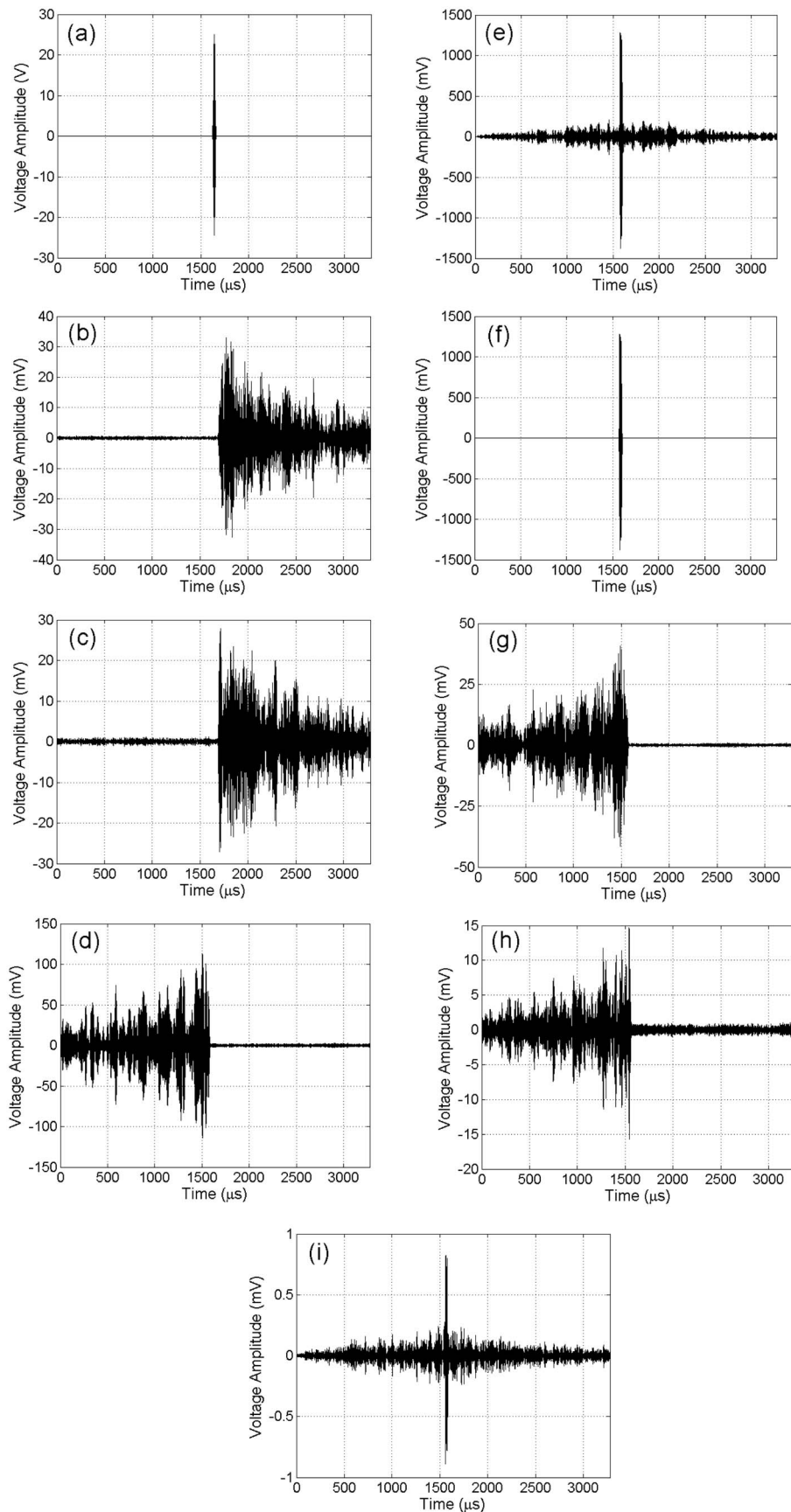
FIG. 3. Subplots (a)–(i) display typical temporal signals used throughout the proposed SSR method. (a) Voltage signal sent to R_i transducers. (b) Signal received at S_1 from transducers R_i. (c) Signal received at S_2 from transducers R_i. (d) Effective TRM signal for R_1 (for first TR step). (e) Focal signal at S_1 (after 1st TR step). (f) Windowed focal signal at S_1 (after first TR step). (g) Effective TRM signal for R_1 (for second TR step). (h) Subtraction result for R_1. (i) Focal signal at S_2 after SSR.

The signals $v_i^{(1+2)}(t)$ contain information from S_1 and S_2. The signals $x_i^{(1)}(t)$ ideally contain information from only S_1. Thus after subtraction to obtain $y_i(t)$, information from only S_2 should remain. In the case of the virtual source experiment, the signals $y_i(t)$ ideally are equivalent to $v_i^{(2)}(t)$. The signals $y_i(t)$ were then time reversed [a typical signal is displayed in

Fig. 3(h)] and broadcast from the TRM transducers into the sample. Once again, the laser vibrometer scans the surface of the sample in the region of interest. To the degree that $y_i(t)$ is similar to $v_i^{(2)}(t)$, a time reversed focus now may be located at S_2. The newly formed focal position corresponds to the original S_2 position. The focal signal $z_2(t)$ [a typical signal is displayed in Fig. 3(i)], detected at S_2, contains a focal waveform that, when windowed appropriately, ideally corresponds to the time reversed version of the original signal $u_2(t)$.

The data taken in this paper utilized a sampling frequency of 10 MHz and signal lengths of 32 768 points or about 3.28 ms. The time of focus was set to be about the center of the 3.28 ms time window, giving 1.64 ms of available data time to collect the direct signal and multiple reflections. The laser vibrometer used in this work consisted of a Polytec OFV 303 sensor head and an OFV 3001 vibrometer controller to measure out-of-plane particle velocity. The envelope of a time waveform is often displayed in the results presented in this paper. The envelope corresponds to the Hilbert transform envelope [envelope=$|S+jH(S)|$, where S is the signal, $j=\sqrt{-1}$, and $H(S)$ is the Hilbert transform of S]. Also, energy located temporally outside of a time reversed focus is referred to as side lobe energy. Side lobes represent the focus being partially recreated before and after the main focal point due to multiply traversed paths within the sample.[23] They must not be confused with the previously cited beamforming side lobes due to the finite spatial sampling of the forward propagation wave fields by an array.

III. RESULTS

A. Blind reconstruction of sources

The SSR method was tested by blind reconstruction of two surficial sources, with one source dominant and the other one weaker (a 5:1 amplitude ratio was used), using the silica glass cube sample (with eight TRM transducers used). A selection of the temporal signals analyzed during the experiment are those reported in Fig. 3.

Le Bas set up the original virtual sources and Anderson carried out the SSR method to locate them. Both sources utilized the same emission time and source characteristics, although their amplitudes were different to ensure masking of the weaker source by the dominant one. Le Bas selected two virtual source locations and an emission time (these were the unknowns for the blind SSR experiment). The source signals themselves, including pulse width and frequency content, were known to both Le Bas and Anderson in the experiment and were carefully selected such that the frequency content allows filtering out of transducer resonances, thus creating a cleaner experiment. However, in the general case, these source characteristics do not need to be known in order to successfully perform SSR since standard TR allows their determination. In addition, the sample surface containing S_1 and S_2 (the scan area, and therefore the potential area for the locations of S_1 and S_2, was limited to a 51 $\times$51 mm^2 to speed up the demonstration) was known to Anderson to eliminate the need to scan all six sides of the cube.
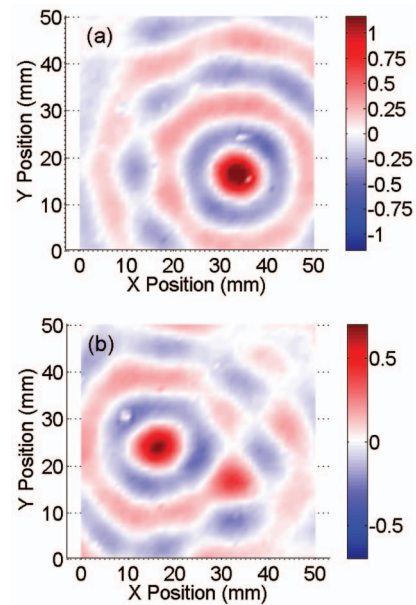

FIG. 4. (Color) Plots of the instantaneous spatial distribution of the (normalized) out of plane velocity at the focal time after standard implementation of the TR process [subplot (a)], and after employing the SSR method [subplot (b)]. A different source is identified in each of the subplots.

Anderson was given only the set of forward received signals $v_i^{(1+2)}(t)$, which were time reversed and broadcast into the medium by the TRM transducers. A laser vibrometer scanned the area of the cube containing the locations of S_1 and S_2. The result of the scanning is displayed in Fig. 4(a), which displays the instantaneous amplitude at the time of focus. The position of S_1 could easily be determined as x =34 mm and y=16 mm, but the position of S_2 could not be determined and was still unknown.

The SSR method was carried out as outlined in Sec. II. As was alluded to previously, filtering of the received signals was used to avoid a significant transducer resonance frequency which was near the center frequency of the source pulses. After performing the SSR method, the laser vibrometer was again used to scan the area of the cube containing the locations of S_1 and S_2. The result of the scanning is displayed in Fig. 4(b) (which displays the instantaneous amplitude at the time of focus). The position of S_2 could now be determined as x=16 mm and y=24 mm. The experimentally determined locations of S_1 and S_2 exactly matched the original virtual source positions determined by the setup person (the scanning resolution was set to be 1 mm for a wavelength of 15.1 mm, thus the actual accuracy was ±0.07 mm).

The focal signals $w_1(t)$ (focal signal at S_1 before SSR) and $z_2(t)$ (focal signal at S_2 after SSR) are plotted in Fig. 5, along with the original source waveform to compare the quality of source reconstruction. Each of the signals displayed in Fig. 5 was normalized to their respective peak values. As one may clearly see, the focal signals are nearly identical to one another. The comparison of the focal signals to the original source signal is quite good, but the focal pulses have a larger pulse width than the original source pulse. This difference is attributed to the fact that the TR process includes an inherent filtering of signals by the me-
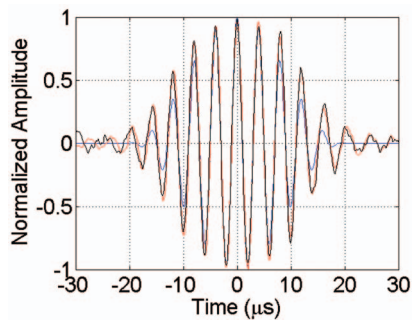
FIG. 5. (Color) Plots of temporal signals to demonstrate the quality of the source reconstruction of TR and of the SSR method. The original source signal is displayed in blue. The focal signal at S_1 after standard TR is displayed in red. The focal signal at S_2 after using the SSR method is displayed in black.

dium and the transducers used and not to an inherent coloration of the SSR method (since the pulse width of the focus at S_1 was wider as well). Essentially, the source pulse passes through the source transducer transfer function, the medium transfer function, and the receiver(s) transfer function(s) both during the forward propagation step and during the back propagation step. If these transfer functions possess frequency dependence, then TR itself will provide a time reversed focus that is not a perfect reconstruction of the source function.

B. Sources in close spatial proximity

An experiment has been conducted on the doped glass block to explore the feasibility of resolving surficial sources spatially located with spacing comparable to a wavelength ($\lambda = 11.7$ mm in the doped glass block). In addition, the results obtained for this section utilized only a single TRM transducer, thus showing the robustness of the SSR method.

In this experiment, using a laser to create virtual sources, one can locate two sources anywhere on the sample surface. Two virtual sources can be spaced at any distance apart, thus two sources can be created such that their centers are located within the *diffraction limit* spot size. The diffraction limit states that a time reversed focus spatial spot size may not be smaller than half the acoustic wavelength.[7,24,25] Note that research has shown that the diffraction limit can be beaten;[6–8,26–29] for example, when one applies an acoustic sink.[7,8]

When sources are very closely located the time reversed foci corresponding to the sources are spatially merged to form one oblong time reversed focus with a peak located in between the actual source positions.[26,30] The degree of elongation of the merged focus depends on how close the two sources are to each other as shown in Fig. 6. The plots in Fig. 6 represent two virtual source TR experiments where the distance between the two, identical in amplitude, virtual sources was varied. The separations of S_1 and S_2 were 8, 6, and 4 mm, respectively, in subplots (a), (b), and (c).

If one had no *a priori* knowledge of the source function and attempted to reduce an oblong source [displayed in Fig. 7(a), which is the same result displayed in Fig. 6(c)] by assuming the source is at the center of the merged result, the
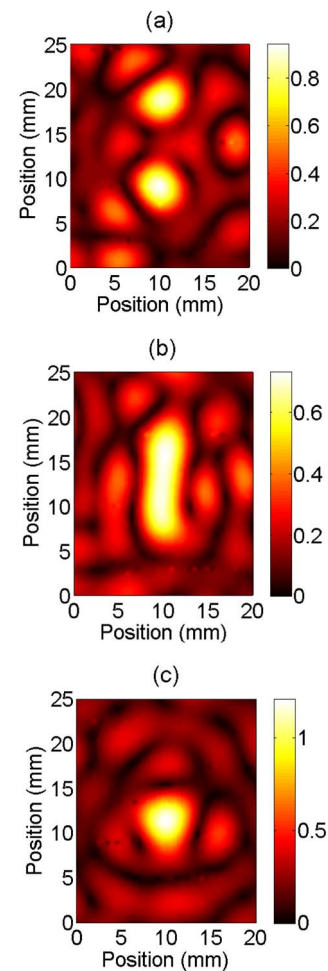

FIG. 6. (Color online) Spatial dependence of the time reversed focal spots which result from progressively decreasing the distance between two sources (virtual sources were used to generate these plots). In subplot (a) the sources are placed 8 mm apart, in subplot (b) they are 6 mm apart, and in subplot (c) they are 4 mm apart (to be compared to the dominant signal wavelength of 11.7 mm). Note the progressive merging of the two focal spots with decreasing separation of sources.

SSR method would produce misleading results as shown in Fig. 7(b). However, if one source location is known the method works, resulting in a circular spatial focus shape at the location of the unknown source as shown in Fig. 7(c). If an oblong time reversed focus is observed but the source locations are unknown, it is conceivable that one could iteratively guess one source location until it is clear that a circular spatial focus has been formed, corresponding to the other source location. Further research must be done to confirm this hypothesis.

IV. DISCUSSION

A. Source reconstruction issues

It has been shown that the time reversed focus of a dominant source may be reduced, thereby providing the means to detect a weaker source. However, as described in the Sec. III A. and demonstrated in Fig. 5, the standard TR process may result in an imperfect reconstruction of the source function. As further evidence of this fact, consider the plots of the envelopes of the time reversed focal signals at S_1
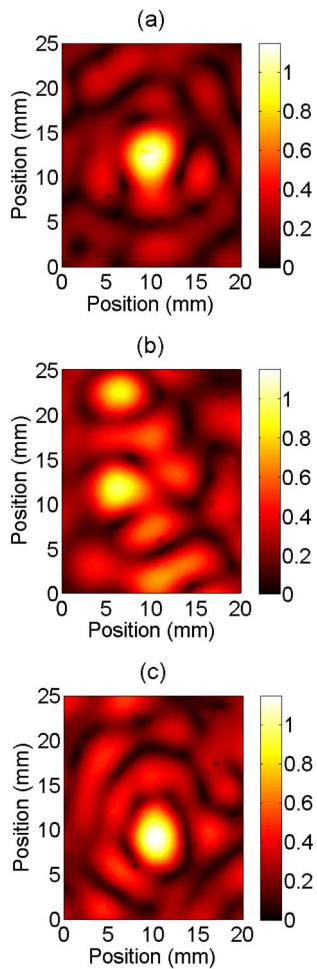
FIG. 7. (Color online) Spatial dependence of the time reversed focal spots generated by two virtual sources separated by 4 mm. Subplot (a) displays the unmodified, merged focal spot. Subplot (b) displays the result of performing SSR on the data in subplot (a) assuming the source is located at the center of the focal spot. Subplot (c) displays the result of performing SSR on the data in subplot (a) with knowledge of the actual location of the upper source: the result is that the lower source location is determined [note that the center of the focal spot shifted vertically from 12 mm down to 10 mm when comparing subplots (a) and (c)].

FIG. 8. (Color) TR focal signals at S_1 (red) and S_2 (black), after using standard TR [subplot (a)] and after using the SSR method [subplot (b)]. The envelope of each signal is displayed.

transducers) is frequency independent. Note that this remnant of focusing at S_1 also occurs in modeling experiments [see Figs. 6(a), 7(a), 9(a), and 10(a) in the paper by Scalerandi *et al.*[9]]. The fact that the remnant is also manifested in modeling results, where the transducers were not included in the model, suggests that an imperfect TR reconstruction can also result in the focusing remnant at S_1.

B. Issues with noise

As a consequence of the issue mentioned in Sec. IV A, the time reversed focus at S_2, after source reduction of S_1, is

(red colored lines) and S_2 (black colored lines), at two stages of the SSR method: after the first TR step [displayed in Fig. 8(a)], and after completing the SSR method [displayed in Fig. 8(b)]. In particular, notice the envelope of the focal signal at S_1 displayed in Fig. 8(b). Notice how there appears to be focusing at S_1 before and after the actual time of focus. Figure 9 displays the instantaneous out-of-plane velocity spatial distribution at the times corresponding to the peaks (in the envelope of the focal signal at S_1) before and after the focal time, displayed in subplots (a) and (b), respectively. The reason for this apparent focusing is due to the imperfect source reconstruction of the source signal at S_1. Consider again the differences between the original source pulse and the focal pulse at S_1 displayed in Fig. 5. Due to the fact that these two pulses are different, the subtraction of the normalized signals $v_i^{(1)}(t)$ and $x_i^{(1)}(t)$ will produce a remnant of focusing at S_1. This remnant is manifested in $y_i(t)$, thus $y_i(t) \neq v_i^{(2)}(t)$. One way to avoid the remnant focusing at S_1 is when a system's transfer function (including the medium and
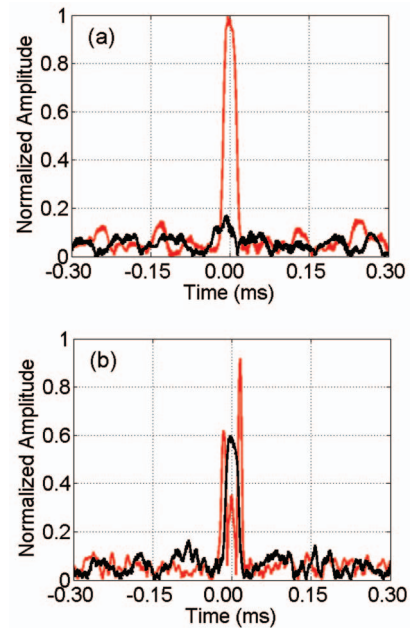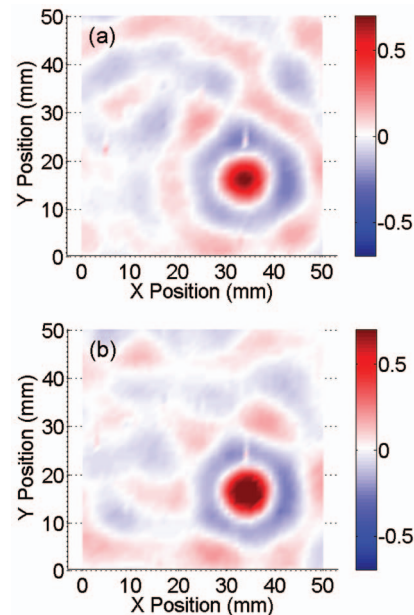

FIG. 9. (Color) Plots of the instantaneous spatial distribution of the out of plane velocity at the times corresponding to the peaks of the signal at S_1 after employing the SSR method, before [subplot (a)] and after [subplot (b)] the time of focus.
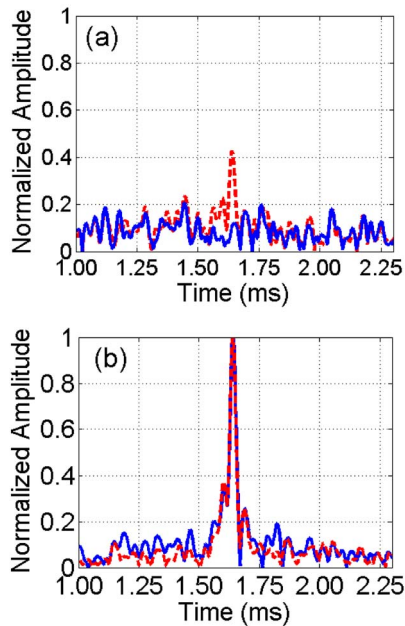
FIG. 10. (Color online) Subplot (a): time reversed focus at S_2 after source reduction with original ratio $A_1/A_2=7.88$ (red line), and time reversed focus at S_2 after source reduction with $A_2=0$ (blue line). Subplot (b): time reversed focus at S_2 after subtraction of the data represented by the blue line from that represented by the red line in subplot (a) (blue line). The time reversed focus detected at S_2 with $A_1=0$ is also displayed (red line). The correlation coefficient of the two signals displayed in the subplot (b) is 91%. The data are normalized with respect to the peak amplitude in subplot (b).

contaminated by spill-over energy arriving at S_1 (this is the remnant after subtraction). If the source reduction technique is performed with no signal originally injected from S_2, then the noise that contaminates the focus at S_2 due to energy intended only for S_1 may be estimated. This noise is obtained by recording the signal at S_2 after performing the source reduction technique on S_1 with no signal injected at S_2. If this noise is subtracted from the time reversed focus at S_2 after source reduction (in situations when S_2 actually injects a signal), then the focus quality at S_2 is greatly enhanced as shown in Fig. 10. This procedure is often not possible in each experimental situation since one may not be able to enable and disable S_2 as desired. This procedure is done here simply to demonstrate further effects of the subtraction remnant, described in Sec. III, that focuses at S_1. As shown in Fig. 10, the reconstruction of S_2 is 91% accurate when the energy intended for S_1 is subtracted.

C. Practical implementation

In this paper, surficial virtual sources were used, which are not realistic representations of an actual blind complex source reconstruction problem, such as in earthquake reconstruction. It is important to note that the authors used virtual sources to demonstrate the SSR method, not to demonstrate the advantages of virtual sources themselves. In the earthquake reconstruction situation using TR, such as was demonstrated by Larmat *et al.*,[1] the initial forward propagation is recorded from actual wave propagation in the Earth. The TR reconstruction of the earthquake must be modeled using an accurate velocity model of the Earth and perform the back-

propagation with a numerical simulation. Under these conditions, SSR, combined with numerical simulations, could be attempted to identify masked earthquake slip events (earthquakes may be considered as a continuous distribution of slip events along the rupturing fault). The focal signal would be extracted from the modeling results and then the forward propagation from that dominant source location would be modeled as well. Assuming similar results in the case of a continuous distribution of emitting sources, the SSR method may potentially yield reconstruction of an approximate rupture history.

As cited in Sec. I, several MF processing techniques have been developed in ocean acoustics for the localization of sources. The basic approach of MF processing consists in comparing the experimental signals recorded at a monitoring array due to the emitting source(s), and the ones generated by numerically modeled source(s) located in test position(s) of the spatial domain under investigation.[12,16] The procedure is iterated moving the test location along a search spatial grid. In this way, an image can be constructed, plotting the comparison metric as a function of the test location (the so-called ambiguity function[12,15]). The actual location of the experimental source corresponds to a maximum location in the ambiguity function, determined using various optimization methods.[30–32] The solution of MF processing is mathematically equivalent to the implementation of a TR procedure. The TR process is a direct way of implementing a spatial and temporal matched filter,[33] that is, a filter which maximizes the signal-to-noise ratio of a scalar field both in time and space.[3,34–36]

MF processing, in its several forms, has been exploited for the localization of multiple sources.[37–39] The main difference between it and the SSR method for sources embedded in the bulk of a medium, like in the earthquake source problem, consists in the total number of numerical simulations required. MF processing requires a large amount of simulations, which is feasible when approximated analytical models of wave propagation are available to reduce the computational burden. This is typical in ocean acoustics problems. On the contrary, for problems such as the localization of earthquake sources in three dimensional (3D), the viscoelastic properties and highly structured heterogeneity of the Earth require solving the full viscoelastic wave equations with the appropriate boundary conditions and modeling of the propagation medium.[1,40] A space parameter direct search is not feasible due to the complexity of the simulations.[41] In theory, the SSR method, by comparison, requires only a limited number of forward and TR backward propagation simulations, the total number depending on the number or sources to be resolved and localized.

In the situation where the entire SSR method may be implemented experimentally, such as in the localization of microcracking on the surface of a sample in NDE applications, the virtual source method may be advantageous. In principle, one could place a transducer at the location of the dominant source in order to obtain the signals $x_i^{(1)}(t)$. However, placement of a transducer in the region of microcracking may inadvertently induce further microcracking or change the structure of the microcracks (by filling them with
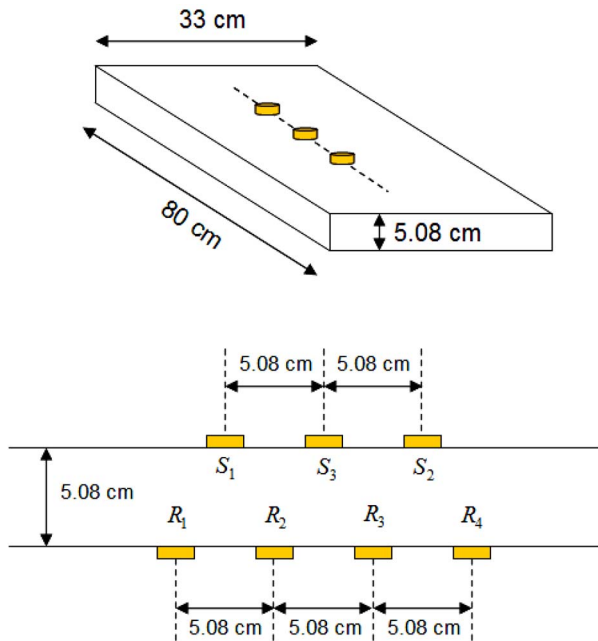
FIG. 11. (Color online) *Schematic of the aluminum slab. S and R represent sources and receivers, respectively.*
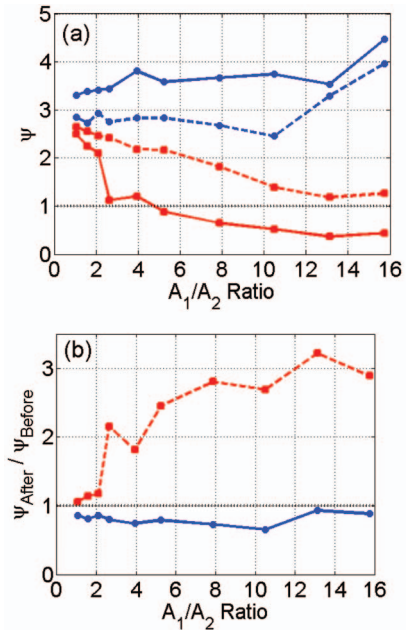

FIG. 12. (Color) Metrics to demonstrate the performance of the SSR method using TR. Subplot (a): amplitude ratio of the peak of time reversed focus to the highest side lobe amplitude ψ for the two sources before and after reduction in the dominant source (S_1) vs the source ratio A_1/A_2. The blue and red lines represent the metric calculated at S_1 and S_2, respectively. The solid and dashed lines refer to before and after source reduction on S_1. Subplot (b): ratio between the metrics calculated before and after the source reduction in S_1 vs the source ratio A_1/A_2. The blue solid line represents the relative decrease in amplitude at S_1 after performing SSR. The red dashed line represents the relative increase in amplitude at S_2 as a result of SSR.

the bonding glue, for example). To avoid the need of placing a transducer at the dominant source location, the virtual source method may be used for surficial interrogation.

In the experiments performed in this work, two surficial virtual sources were used to demonstrate the SSR method. However, *a priori* knowledge of the number of original sources is not required. For example, in the blind source reconstruction problem, it is conceivable that the SSR method could be performed again in an attempt to reduce the focus at S_2, thus allowing the localization and characterization of a third masked source (assuming that the noise floor would not prevent this possibility). Furthermore, the remnants at S_1 may be iteratively reduced, although this has not been yet experimentally verified.

Finally we observe that, if in the first place there was only one source event then one would obviously not find a masked source event. The SSR method simply allows one to check whether there are multiple source events which have been masked by the standard TR process.

V. LIMITATIONS

The SSR method will work only in a limited range of amplitude ratios between the two sources (due to effects like those discussed in Sec. IV). To investigate the limits in the performance of the method, a third experiment has been performed on an aluminum slab sample (schematically depicted in Fig. 11) by using real sources. Both transducers acting as sources (S_1 and S_2) and transducers acting as receivers (R_i) are 1 MHz resonance PZT-5H ceramic transducers disks measuring 2.0 mm in thickness and with 12.7 mm diameter. They were bonded to the sample in the same vertical plane, but shifted relative to each other such that no transducer was directly across from another.

The SSR method has been applied to reduce S_1 (dominant source) along with varying the ratio of the sources am-

plitudes A_1/A_2. A signal-to-noise metric ψ was introduced to monitor the quality of the time reverse focal signal. ψ is defined as the ratio of the peak of the time reverse focal envelope amplitude (peak near focal time) to the peak envelope amplitude of the highest side lobe. For example, a ratio of 1.0 corresponds to no focal signal, whereas a ratio of 5.0 means that the focal signal is five times higher than the highest side lobe.

Figure 12(a) displays the calculated metric for the time reverse focal signal at the two sources before and after performing the SSR technique. The ratio of the metrics before and after applying the SSR method ($\psi_{after}/\psi_{before}$) is also reported in Fig. 12(b) for the two sources. The metric for the dominant source is always decreased by the application of the source reduction [compare the blue solid and dotted lines in Fig. 12(a)], even though the focus amplitude is never decreased to the noise floor level (the two peaks emerging after source reduction have been considered in the calculation as part of the focus and not side lobes). ψ for the secondary source S_2 is always larger after source reduction [solid and dashed red lines in Fig. 12(a)]. The ratio of the metrics before and after source reduction [Fig. 12(b)] is approximately constant for S_1, while it increases for S_2 with the input source ratio up to a ratio of 13 and then it falls off as the input ratio increases further. The dip at an input ratio of 3.94 is unknown and perhaps due to experimental causes.

From the data displayed in Fig. 12(a), it is apparent that the standard TR approach brings the focus at S_2 out of the side lobes level only up to an input amplitude ratio of about

2, while the SSR procedure allows to bring the focus at S_2 out of the noise level up to $A_1/A_2=11$. At larger values of the input ratio, the focus at S_2 is just above its side lobe noise level, hence we have shown the existence of the limit for the procedure adopted.

The focal signals were recorded by the respective source transducers for this set of experiments, thus utilizing *a priori* information. This set of experiments may not yield the same limitations as would be encountered with the type of experiment conducted for the blind sources test of Sec. III A. The limitations on the success of the SSR method, considering the initial ratio of A_1/A_2, will vary according to many parameters of the experiment, such as noise floors and transducer sensitivities. Thus the intent of the experiments presented in this section is to give the reader a clear indication that such a limit exists in all applications of this method in the initial ratio of A_1/A_2. A similar analysis conducted on the doped glass cube has indicated a limit ratio $A_1/A_2=4$. This poor ratio was, in our opinion, due to the poor signal-to-noise ratio given by the use of small transducers, which cannot transmit energy as well as the transducers used in the aluminum sample. In addition, the use of the laser vibrometer in the doped glass block imposed additional noise floor issues.

The implementation of SSR for localizing sources in 3D is highly affected by the uncertainties in modeling the elastic wave propagation through the medium/specimen. Reliable source localization and parameter estimation are only possible when the propagation medium/specimen parameters are known with high degree of accuracy.[42] This is particularly true in the presence of multiple scattering or multiple reflections at boundaries.[43] It is an intrinsic limitation of any imaging method exploiting modeling and numerical simulation of elastic wave propagation in an uncertain environments.[44] MF processing methods are affected by the same type of problem.[45–49]

VI. CONCLUSIONS

This paper has provided important experimental verifications of the SSR method using TR, which was proposed by Scalerandi *et al.*[9] It has been shown that a weaker secondary source, which is masked by a stronger dominant source, may be illuminated, by employing the SSR method, based on subtraction of the dominant source direct arrival and coda. SSR has application in the detection of complex microcrack distributions in mechanical parts (NDE of solid materials) and possibly in the spatial/temporal characterization of complex earthquake sources.

A blind surficial source reconstruction experiment conducted in this work successfully shows that SSR may be performed despite not knowing either the source positions or their time of emission. Thus this method provides a means of resolving masked sources in a complex source problem without prior knowledge of the source function(s) and/or without modification of the sample.

The SSR method is limited by the source reconstruction ability of the TR process. In addition, when two sources are emitted in close spatial proximity, relative to the wavelength,

the location of one of the two sources must be known in order to characterize both sources. However, it is proposed that an iterative guessing of the location of one of the sources may allow characterization of both sources, although not proven in this work.

[1] C. Larmat, J.-P. Montagner, M. Fink, Y. Capdeville, A. Tourin, and E. Clevede, Geophys. Res. Lett. **33**, L19312 (2006).
[2] C. Prada, E. Kerbrat, D. Cassereau, and M. Fink, Inverse Probl. **18**, 1761 (2002).
[3] I. Tolstoy and C. Clay, *Ocean Acoustics. Theory and Experiment in Underwater Sound* (McGraw-Hill, New York, 1966), Chap. 7, pp. 243–268.
[4] M. Fink, Phys. Today **50**, 34 (1997).
[5] B. E. Anderson, M. Griffa, C. Larmat, T. J. Ulrich, and P. A. Johnson, Acoust. Today **4**, 5 (2008).
[6] G. Lerosey, J. de Rosny, A. Tourin, and M. Fink, Science **315**, 1120 (2007).
[7] D. Cassereau and M. Fink, IEEE Trans. Ultrason. Ferroelectr. Freq. Control **39**, 579 (1992).
[8] J. de Rosny and M. Fink, Phys. Rev. Lett. **89**, 124301 (2002).
[9] M. Scalerandi, A. S. Gliozzi, B. E. Anderson, M. Griffa, P. A. Johnson, and T. J. Ulrich, J. Phys. D: Appl. Phys. **41**, 155504 (2008).
[10] B. D. Steinberg, *Principles of Aperture and Array System Design* (Wiley, New York, 1976).
[11] J. A. Högbom, Astron. Astrophys. **15**, 417 (1974).
[12] A. B. Baggeroer, W. A. Kuperman, and H. Schmidt, J. Acoust. Soc. Am. **83**, 571 (1988).
[13] B. D. Steinberg, *Microwave Imaging with Large Antenna Arrays* (Wiley, New York, 1983).
[14] H. P. Bucker, J. Acoust. Soc. Am. **59**, 368 (1976).
[15] M. J. Hinich, J. Acoust. Soc. Am. **66**, 480 (1979).
[16] A. B. Baggeroer, W. A. Kuperman, and P. N. Mikhalevsky, IEEE J. Ocean. Eng. **18**, 401 (1993).
[17] J. Tsao and B. D. Steinberg, IEEE Trans. Antennas Propag. **36**, 543 (1988).
[18] H. C. Song, J. de Rosny, and W. A. Kuperman, J. Acoust. Soc. Am. **113**, 1379 (2003).
[19] J. W. S. Rayleigh, *The Theory of Sound*, 1st ed. (Macmillan, London, 1877), Vol. I, Chap. XIV, pp. 145–147; *The Theory of Sound*, 1st ed. (Macmillan, London, 1878), Vol. II; *The Theory of Sound*, 2nd ed. (Macmillan, London, 1894), Vol. I; *The Theory of Sound*, 2nd ed. (Macmillan, London, 1896), Vol. II.
[20] L. Knopoff and A. F. Gagni, Geophysics **24**, 681 (1959).
[21] L. E. Kinsler, A. R. Frey, A. B. Coppens, and J. V. Sanders, *Fundamentals of Acoustics*, 4th ed. (Wiley, New York, 1982), Chap. 7, pp. 172–176.
[22] J. D. Achenbach, *Reciprocity in Elastodynamics* (Cambridge University Press, Cambridge, 2003), Chap. 1.
[23] C. Draeger and M. Fink, Phys. Rev. Lett. **79**, 407 (1997).
[24] R. P. Porter and A. J. Devaney, J. Opt. Soc. Am. **72**, 327 (1982).
[25] R. P. Porter, J. Opt. Soc. Am. **60**, 1051 (1970).
[26] F. Simonetti, *Annual Review of Quantitative Nondestructive Evaluation* (American Institute of Physics, Melville, 2006), Vol. 820, p. 700.
[27] F. Simonetti, Phys. Rev. E **73**, 036619 (2006).
[28] A. Derode, P. Roux, and M. Fink, Phys. Rev. Lett. **75**, 4206 (1995).
[29] C. Prada and J. Thomas, J. Acoust. Soc. Am. **114**, 235 (2003).
[30] M. D. Collins and W. A. Kuperman, J. Acoust. Soc. Am. **90**, 1410 (1991).
[31] P. Gerstoft, J. Acoust. Soc. Am. **95**, 770 (1994).
[32] S. E. Dosso, J. Acoust. Soc. Am. **111**, 129 (2002).
[33] G. L. Turin, IRE Trans. Inf. Theory **6**, 311 (1960).
[34] C. Dorme and M. Fink, J. Acoust. Soc. Am. **98**, 1155 (1995).
[35] M. Tanter, J.-L. Thomas, and M. Fink, J. Acoust. Soc. Am. **108**, 223 (2000).
[36] D. H. Chambers, J. V. Candy, S. K. Lehman, J. S. Kallman, A. J. Poggio,

and A. W. Meyer, J. Acoust. Soc. Am. **116**, 1348 (2004).

[37] M. D. Collins, L. T. Fialkowski, W. A. Kuperman, and J. S. Perkins, J. Acoust. Soc. Am. **97**, 235 (1995).

[38] M. V. Greening, P. Zakarauskas, and S. E. Dosso, J. Acoust. Soc. Am. **101**, 3525 (1997).

[39] Z.-H. Michalopoulou, J. Acoust. Soc. Am. **120**, 2627 (2006).

[40] D. Komatitsch, J. Ritsema, and J. Tromp, Science **298**, 1737 (2002).

[41] V. Akçelik, G. Biros, and O. Ghattas, Proceedings of the ACM/IEEE Supercomputing SC'2002 Conference (unpublished), available at www.sc-conference.org/sc2002.

[42] K. Mehta and R. Snieder, Am. J. Phys. **74**, 224 (2006).

[43] G. Bal and R. Verstegui, Multiscale Model. Simul. **2**, 639 (2004).

[44] J. A. Scales and R. Snieder, Geophysics **62**, 1355 (1997).

[45] D. R. Del Balzo, J. Acoust. Soc. Am. **83**, 2180 (1988).

[46] A. Tolstoy, J. Acoust. Soc. Am. **85**, 2394 (1989).

[47] D. F. Gingras, J. Acoust. Soc. Am. **86**, 1940 (1989).

[48] R. M. Hamson and R. M. Heitmeyer, J. Acoust. Soc. Am. **86**, 1950 (1989).

[49] H. Schmidt, A. B. Baggeroer, W. A. Kuperman, and E. K. Scheer, J. Acoust. Soc. Am. **88**, 1851 (1990).